Fort Lauderdale, Florida
NOISE-CON 2014
2014 September 8–10

Transmission loss and absorption of corrugated core sandwich panels with embedded resonators

Albert R. Allen
Noah H. Schiller
NASA LaRC, Mail Stop 463
Hampton, VA 23681 USA
albert.r.allen@nasa.gov
noah.h.schiller@nasa.gov

Bart F. Zalewski
Zin Technologies, Inc.
Cleveland, OH 44130 USA
zalewskib@zin-tech.com

Bruce N. Rosenthal
NASA GRC, Mail Stop 86-1
Cleveland, OH 44135 USA
bruce.n.rosenthal@nasa.gov

ABSTRACT

The effect of embedded resonators on the diffuse field sound transmission loss and absorption of composite corrugated core sandwich panels has been evaluated experimentally. Two 1.219 m $\times$ 2.438 m panels with embedded resonator arrangements targeting frequencies near 100 Hz were evaluated using non-standard processing of ASTM E90-09 acoustic transmission loss and ASTM C423-09a room absorption test measurements. Each panel is comprised of two composite face sheets sandwiching a corrugated core with a trapezoidal cross section. When inlet openings are introduced in one face sheet, the chambers within the core can be used as embedded acoustic resonators. Changes to the inlet and chamber partition locations allow this type of structure to be tuned for targeted spectrum passive noise control. Because the core chambers are aligned with the plane of the panel, the resonators can be tuned for low frequencies without compromising the sandwich panel construction, which is typically sized to meet static load requirements. Absorption and transmission loss performance improvements attributed to opening the inlets were apparent for some configurations and inconclusive for others.

1. Introduction

A launch vehicle interior noise control concept currently of interest involves the integration of large wavelength tuned chamber core resonators within a corrugated core structural sidewall. This concept takes advantage of the existing core chamber volumes, whereby inlets are introduced at particular locations on the interior face sheet to create an array of acoustic resonators. A schematic of this structural concept with integrated acoustic resonators is shown in Figure 1. Noise control is achieved by both reducing the transmission of sound through the panel and increasing the absorption within the vehicle interior acoustic volume. For a given application, it is envisioned that the chamber and inlet geometries would be tailored to provide a desired noise reduction (NR) spectrum while also maintaining load bearing capabilities.

The embedded resonator noise control concept has been a topic of previous interest for space launch vehicle and commercial aircraft applications. In 1991, Kuntz et al. described the development and testing of add-on hemispherical resonators to reduce cabin noise in propfan-powered aircraft [1]. In one configuration the resonators were installed in the cavity between the sidewall and trim panel to attenuate the double wall resonance of the system. In this case a noise reduction of more than 10 dB was observed in laboratory experiments. Subsequent work considered the benefit of embedding acoustic resonators into the wall of a space launch vehicle payload fairing [2, 3]. Specifically, the fairing consisted of two facesheets separated by a hollow core with long rectangular chambers used as the acoustic resonators. The benefit of this concept is that the double wall structure is strong and lightweight and includes acoustic resonators without the additional volume or weight

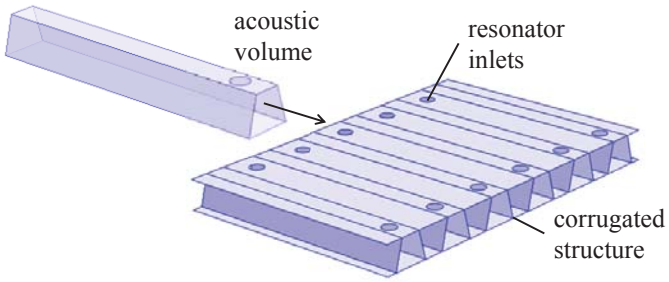

Figure 1: Corrugated core panel with integrated resonators.

of add-on resonators. Li et al. showed that the integrated resonators could effectively attenuate low-frequency acoustic resonances [4]. The Space Launch System payload fairing structure has recently undergone a trade study that included the corrugated sandwich concept [5]. The team ultimately recommended a honeycomb sandwich architecture as the point of departure design. However, the study was performed without accounting for the acoustic benefit of resonators within the corrugated sandwich structure. If the embedded resonators can be used to attenuate low frequency noise, then the corrugated sandwich concept may provide better overall performance than alternative architectures due to weight savings resulting from a reduced need for thick acoustic foam treatment.

Absorption and transmission loss tests were conducted on several integrated resonator corrugated core test articles at Riverbank Acoustical Laboratories (RAL) in Geneva, IL from April 9-11, 2014. Due to the expected narrowband performance of the integrated resonators and their *apriori* unknown quality factors, time histories of all tests were acquired for subsequent analysis over band bases narrower than the standard 1/3 octave band basis. In the following section, the test articles are described. This is followed by a description of the post processing techniques applied to the acquired time histories, and a discussion of the experimental results.

2. Test Articles

Three types of corrugated core panels with varied thickness and corrugation patterns were initially fabricated. The panel thicknesses were 25.4 mm, 50.8 mm, and 101.6 mm, denoted as P1, P2, and P4. However, only P2 and P4 configurations were tested during this investigation due to mid-test reprioritization. Each 1.22 m $\times$ 2.44 m panel was fabricated in three 1.22 m $\times$ 0.81 m sections. These subpanels were then placed adjacent to one another during TL and absorption testing. Geometrical details of the P2 and P4 subpanel constructions are shown in Table 1. The P2 and P4 inlet diameters were machined to 25.4 mm and 50.8 mm, respectively. The application of 25.4 mm inner diameter aluminum annular discs to the P4 inlets allowed for an additional P4 configuration with reduced inlet diameters.

Initially the subpanels were not sealed at the ends so that the 0.81 m long chambers within the core could be visually inspected. However, to be effective as an acoustic resonator, the chambers had to be sealed on both ends while leaving a single inlet in the top face sheet. This was realized by adhering carbon laminate strips to either side of the subpanels along the 1.22 m long cross sections with butyl sealant tape. This provided an air tight seal at the top and bottom of each resonator. The chamber lengths of P2 were reduced during the latter phase of testing by replacing the taped laminate endcaps with approximately 25.4 mm deep closed cell foam plugs that inserted into the chambers, conforming to the trapezoidal chamber cross section. The foam plugs were used to create 356 mm long chambers, as measured from endcap-to-endcap. In hindsight, the closed cell foam plugs provided a much simpler endcap solution in terms installation, adjustability, and removal.

3. Test Procedures

The RAL facilities that were utilized in this test consisted of a large 291 m^3 reverberant room for absorption measurements (Room 0) and dual 178 m^3 (source, Room 2) and 139 m^3 (receive, Room 3) reverberant rooms coupled through (at most) a 1.22 m $\times$ 2.44 m opening for the measurement of diffuse acoustic field transmission

Table 1: Geometric details of P2 and P4 subpanels (unit = mm).

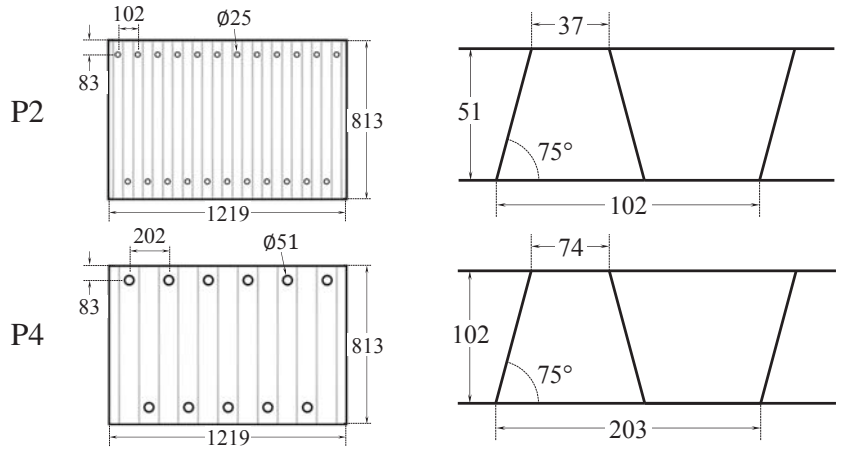

loss. Each room included a corner located sound source as well as static and rotating diffusers to promote sound field diffusivity. During testing, pressure signals were acquired with a single 12.7 mm diameter diffuse field microphone on a centrally located rotating boom.

The absorption tests were conducted in Room 0 in conformance with the requirements of ASTM C423-09a, whereby the room absorption area is determined by averaging the band limited reverberation decay rates resulting from a series of microphone-measured noise burst and decay events [6]. The absorption area was then calculated using the Sabine formula, $A = 0.9210(Vd/c)$, where d is the dB/s decay rate after subtracting out the decay rate due to air absorption and V and c are the room volume and speed of sound, respectively. Ambient room dry bulb temperature and relative humidity were recorded at the beginning and end of each absorption measurement and were used to determine air absorption per ANSI S1.26 [7].

The standard absorption test procedure involves the measurements of A with and without the test article placed on the floor to determine the absorption area attributed to the test article. In this case, however, two absorption measurements consisting of the panel placed in the room with and without inlets covered were used to ascertain the performance of the embedded resonator array. The room noise reduction due to resonator absorption can then be written as

$$NR = 10\log_{10}\left(A/A_0\right), \tag{1}$$

where A and A_0 are the room absorption areas with open and closed resonator inlets, respectively.

Images of the P2 and P4 open inlet absorption test configurations are depicted in Figure 2. To cover the inlets, 0.18 mm thick aluminum tape was adhered over the inlets. Prior experimental efforts have shown this method of inlet closing to be adequate. Because this is a resonant noise control concept and because the summed inlet areas were largely insufficient when considering the C423-09a size and shape requirements, determination of an absorption *coefficient* was of little interest and only the room absorption area was considered for the purposes of performance assessment and model correlation.

The ASTM E90-09 TL tests carried out in Room 2 and Room 3 consisted of measuring the three right hand side terms of the expression

$$TL = \langle L_1 \rangle - \langle L_2 \rangle + 10\log_{10}\left(S/A_2\right), \tag{2}$$

where $\langle L_1 \rangle$ and $\langle L_2 \rangle$ refer to the average sound pressure level in the source and receive room, S is the surface area of the test panel facing the receive room, and A_2 is the receive room absorption area [8]. The receive room absorption area A_2 was measured corresponding to the aforementioned absorption measurement procedure, although in this case the air absorption effects were not removed from the decay rates. Room levels $\langle L_1 \rangle$

(a) P2, 25.4 mm dia. inlets (b) P4, 25.4 mm dia. inlets (c) P4, 50.8 mm dia. inlets

Figure 2: Absorption test cases.

and $\langle L_2 \rangle$ were subsequently measured during serial acquisitions while the source room was ensonified with steady-state broadband noise. The space and time average room levels were determined from 160 second long acquisitions corresponding to 5 revolutions of the rotating microphone.

TL tests for each configuration were performed with open and closed inlets to determine the Insertion Loss (IL) attributed to opening the resonator inlets on the radiating side of the panel. Use of the IL to assess the noise control capabilities of the embedded resonators avoided the difficulty of accounting for the complex structural dynamics of the corrugated core construction as well as the uncertain boundary conditions at the subpanel perimeters. This approach assumes 1) no change in the structure from open to closed inlet configurations, and 2) the vibroacoustic coupling within the resonator is a component of the resonator influence and is accounted for during performance assessment and model correlation. The assumption of no change between open and closed TL tests was found to be reasonable given that the only difference introduced between tests was the addition or removal of aluminum tape covers comprising 1% or less of the total panel mass. Images of the P2 and P4 open inlet TL test configurations are depicted in Figure 3. The subpanels were stacked end-to-end in the opening between the source and receive rooms during these tests. Only 2 of the 3 subpanels were installed during the P4 TL tests due to insufficient clearance in the test window.

(a) P2, 25.4 mm dia. inlets (b) P4, 25.4 mm dia. inlets (c) P4, 50.8 mm dia. inlets

Figure 3: Transmission loss test cases.

Due to the expected narrowband performance of the resonators, time histories were acquired during all tests for post processing within band bases narrower than 1/3 octave. For example, 160 second steady state noise time histories were acquired in the source and receive rooms during the E90-09 TL tests. Also, 600 seconds of burst and decay events were acquired during the C423-09a absorption measurements (and E90-09 TL receive room absorption measurements). This acquisition length included a sample size of approximately 50 bursts, which was deemed adequate for the estimation of absorption area mean and confidence intervals. These time histories were acquired during the standard measurements with a separate data acquisition system (NI USB-4431) connected to the microphone through a LEMO cable splitter. The introduction of the LEMO splitter to the existing acquisition system was vetted prior to testing to avoid any undesirable effects on the standard measurements.

4. Data reduction and results

A. Absorption

A band-limited reverse integration method was applied to the absorption test burst/decay time histories to estimate the average room decay rate and reverberation time spectra using various band bases. During this process, the following steps were carried out on the acquired 600 second absorption test time histories:

1) Approximately 50 burst and decay events were segmented and temporally aligned using a window and gating technique.
2) The burst events were filtered using 1/n octave filter banks of 6$^{\text{th}}$ order Butterworth bandpass filters conforming to at least Class 1 filter shape specifications in ANSI S1.11 [9].
3) Decay envelopes $p_{env}(t)$ were determined from the resulting N-length band limited decay time histories $p(t)$ using a normalized reverse integrated Schroeder decay method expressed as $p_{env}(t) = 1 - \left(\sum_{s=0}^{t} p^2(s)\right) / \left(\sum_{s=0}^{N} p^2(s)\right)$.
4) Linear regressions of the dB decay envelopes were performed resulting in sets of band limited decay rates used to determine reverberation times and absorption areas.

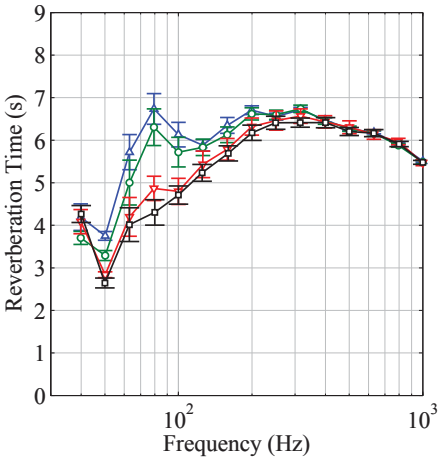

Figure 4: Empty room 1/3 octave reverberation time spectra with 95% confidence intervals from processed burst time histories determined using T30 (▵), T20 (○), and EDT (▽) curve fitting methods compared with C423-09a test results (▫).

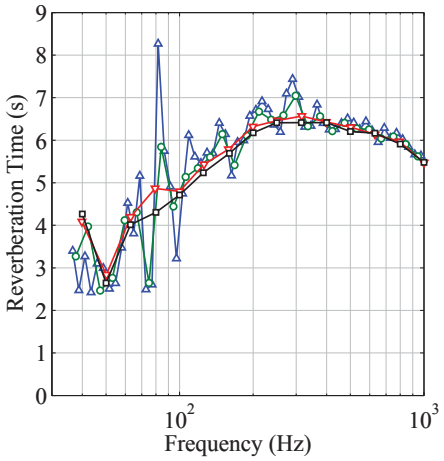

Figure 5: Empty room EDT reverberation time spectra from processed time histories determined using 1/12 (▵), 1/6 (○), and 1/3 (▽) octave band bases compared with 1/3 octave C423-09a test results (▫). Confidence intervals not shown for readability.

The 95% confidence intervals of the mean absorption area were determined using $A \pm k\left(s/\sqrt{N}\right)$ with a coverage factor of $k = 2$, where s is the standard deviation and N is the burst sample size of approximately 50.

The reverberation times determined this way were initially evaluated on a 1/3 octave band basis using different methods including EDT, T20, and T30 reverberation times ([0, -10], [-5, -25], and [-5 -35] dB decay fit ranges, respectively) and compared with results from the C423-09a test results, an example of which is shown in Figure 4. The EDT results were found to be in much better agreement with the C423-09a results relative to T20 and T30 results for all absorption test cases, especially at lower frequencies, and were consequently used for the remaining analyses. The process was then performed using narrower 1/6 and 1/12 octave band bases as shown in Figure 5, where the effect of room modes becomes more apparent at finer spectral resolutions, especially at lower frequencies.

The 1/6 octave band absorption results for the three absorption test cases evaluated using equation 1 are shown in Figure 6. The 1/6 band basis adequately resolved the peak and bandwidth characteristics of the resonators while avoiding the larger uncertainty (wider confidence intervals) inherent to the 1/12 octave band results. Peaks in the P2 absorption spectra are evident near 100 Hz and to a lesser extend near 300 Hz and 500 Hz. Although the embedded resonators are not ideal quarter wave resonators, the spacing of the peaks is representative of the odd multiples of the quarter wave resonator harmonics. Similarly, the P4, 25.4 mm inlet absorption spectrum exhibits peaks near 70 Hz and 210 Hz. While there was no change in chamber length between P2 and P4, the larger chamber cross-section and vibroacoustic coupling with the thin laminate chamber walls likely contributed to a reduced resonant frequency. Slight resonant characteristics near 70-100 Hz and 200-300 Hz were noticed in the P4, 50.8 mm inlet results, although the effects were not substantial and are inconclusive. This may be due to poor coupling between the low frequency room modes and the embedded resonators for the given test article placement and natural frequency of the resonators.

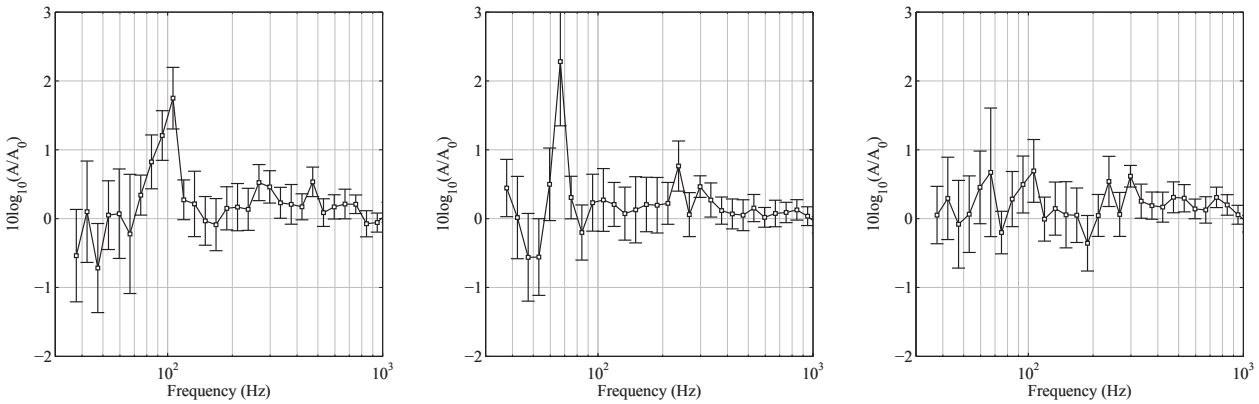

(a) P2, 25.4 mm dia. inlets (b) P4, 25.4 mm dia. inlets (c) P4, 50.8 mm dia. inlets

Figure 6: 1/6 octave band absorption performance for the three absorption test cases shown in Figure 2. 95% Confidence intervals shown are the combined open and closed inlet absorption area dB uncertainties.

B. Transmission

As previously described, transmission loss is calculated based on measurements of source room level, receive room level, and receive room absorption per equation 2. The receive room absorption component was computed from burst decay time histories measured in the receive room using the previously described method. The following steps were carried out to process the 160 seconds of steady state room level time histories:

1) The first 5 seconds of data was discarded to allow the room level to reach steady-state.

2) The data was divided into 5 equal blocks that were each 31 seconds long.
3) The 31 second blocks were filtered using 1/n octave filter banks of 6^{th} order Butterworth bandpass filters conforming to at least Class 1 filter shape specifications in ANSI S1.11 [9].
4) The band limited room levels were determined from the band limited time history root mean square pressures calculated as $p_{rms} = \sqrt{\frac{1}{N}\sum_{s=1}^{N}|p\,(s)|^2}$.

The mean and standard deviation of the average sound pressure level in the source and receive rooms were calculated this way for the 5 blocks of data and the corresponding 95% confidence intervals were estimated. The mean transmission loss was then calculated using equation 2 and the 95% confidence intervals were found using Equation A2.5 in ASTM E90-09. The TL determined in this way was initially evaluated on a 1/3 octave band basis and was found to compare favorably with the E90-09 test results. The process was then performed using narrower 1/6 octave band bases and the IL due to opening the resonator inlets was determined as shown in Figure 7.

Unfortunately, the full chamber length P2 and P4 configuration IL results were largely inconclusive. The P4 results also exhibited consistent negative IL near 350 Hz, which may be due to interactions between the structural dynamics and resonator acoustic volume. However, a positive IL near 200 Hz was evident in the IL results from the P2 configuration with reduced chamber lengths.

5. Conclusions

An experimental assessment of the absorption and transmission loss performance of the corrugated core embedded resonator noise control concept has been carried out on test panels including different thicknesses, corrugation geometries, and inlet diameters. Post processing of microphone time histories acquired during standard ASTM E90-09 transmission loss and C423-09a absorption tests were used to resolve resonator characteristics using band bases narrower than 1/3 octave. The relative performance attributed to opening the resonator inlets was then evaluated using measures of the dB ratio of absorption areas and change in transmission loss. Resonant characteristics were noticed in the absorption and transmission loss results for some configurations, while other configurations showed inconclusive results attributable to strong room mode interactions (or lack thereof) at lower frequencies. Follow-up tests conducted using these test articles are slated for the near future to explore further panel configurations and different test procedures aimed at improved characterization of low frequency resonant noise control concepts.

6. Acknowledgements

The authors gratefully acknowledge the support of Anne McNelis, Bill Hughes, and the RAL technicians during testing, and are also grateful to Justin Jackson for his role in panel fabrication.

REFERENCES

[1] H. L. Kuntz, R. J. Gatineau, R. A. Prydz, and F. J. Balena. Development and testing of cabin sidewall acoustic resonators for the reduction of cabin tone levels in propfan-powered aircraft. Technical Report CR 4388, NASA, 1991.

[2] S. A. Lane, R. E. Richard, and S. J. Kennedy. Fairing noise control using tube-shaped resonators. *Journal of Spacecraft and Rockets*, 42:640–646, 2005.

[3] S. A. Lane, K. Henderson, A. Williams, and E. Ardelean. Chamber core structures for fairing acoustic mitigation. *Journal of Spacecraft and Rockets*, 44:156–163, 2007.

[4] D. Li and J. S. Vipperman. Noise control of mock-scale chambercore payload fairing using integrated acoustic resonators. *Journal of Spacecraft and Rockets*, 43:877–882, 2006.

[5] T. M. Krivanek and B. C. Yount. Composite payload fairing structural architecture assessment and selection. In *Proceedings of the Society for the Advancement of Material and Process Engineering Conference*, Baltimore, MD, May 2012.

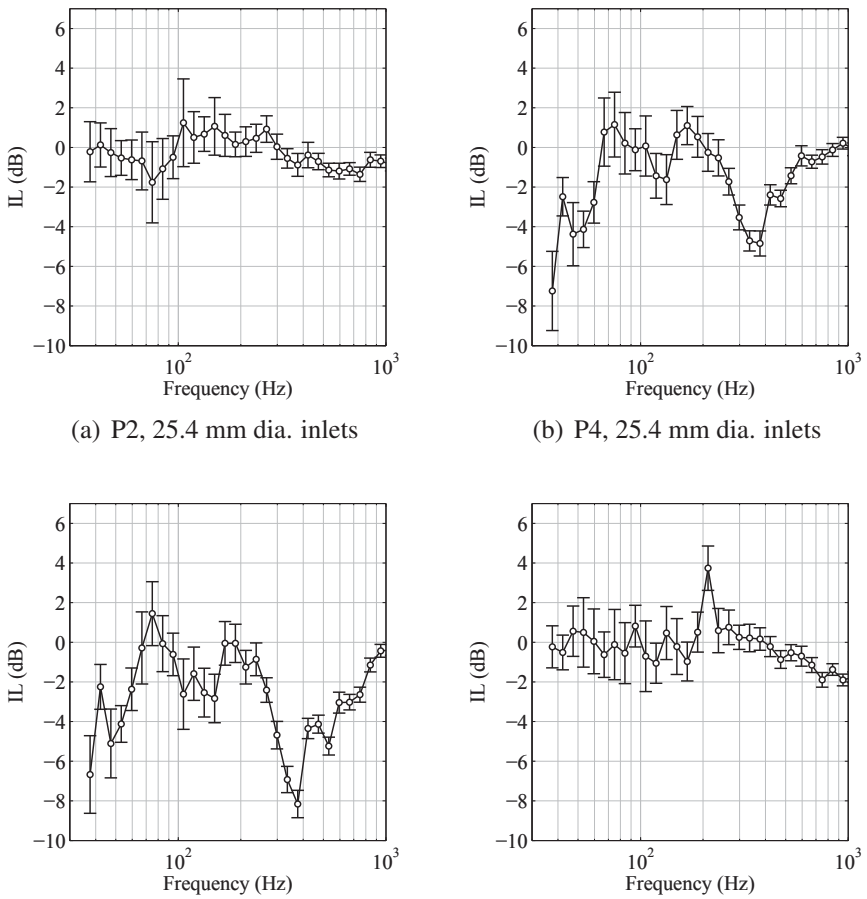

(a) P2, 25.4 mm dia. inlets

(b) P4, 25.4 mm dia. inlets

(c) P4, 50.8 mm dia. inlets

(d) P2, 25.4 mm dia. inlets, reduced chamber lengths

Figure 7: 1/6 octave band IL due to open inlet resonators for the three TL test cases shown in Figure 3. 95% Confidence intervals shown are the combined open and closed inlet TL dB uncertainties.

[6] ASTM C423-09a. *Standard Test Method for Sound Absorption and Sound Absorption Coefficients by the Reverberation Room Method*, 2009.

[7] ANSI S1.26-1995 (R2009). *Calculation of the Absorption of Sound by the Atmosphere*, 2009.

[8] ASTM E90-09. *Standard Test Method for Laboratory Measurement of Airborne Sound Transmission Loss of Building Partitions and Elements*, 2009.

[9] ANSI S1.11-2004 (R2009). *Specification for octave-band and fractional-octave-band analog and digital filters*, 2009.